OPEN ACCESS
IOP Publishing
Journal of Physics: Condensed Matter
J. Phys.: Condens. Matter **27** (2015) 315701 (9pp)
doi:10.1088/0953-8984/27/31/315701

Observability of surface Andreev bound states in a topological insulator in proximity to an *s*-wave superconductor

M Snelder[1], A A Golubov[1,2], Y Asano[3] and A Brinkman[1]

[1] Faculty of Science and Technology and MESA+ Institute for Nanotechnology, University of Twente, 7500 AE Enschede, The Netherlands
[2] Moscow Institute of Physics and Technology, Dolgoprudny, Moscow 141700, Russia
[3] Department of Applied Physics and Center for Topological Science & Technology, Hokkaido University, Sapporo 060-8628, Japan

E-mail: a.brinkman@utwente.nl

Received 28 April 2015, revised 2 June 2015
Accepted for publication 17 June 2015
Published 20 July 2015

Abstract

To guide experimental work on the search for Majorana zero-energy modes, we calculate the superconducting pairing symmetry of a three-dimensional topological insulator in combination with an *s*-wave superconductor. We show how the pairing symmetry changes across different topological regimes. We demonstrate that a dominant *p*-wave pairing relation is not sufficient to realise a Majorana zero-energy mode useful for quantum computation. Our main result is the relation between odd-frequency pairing and Majorana zero energy modes by using Green functions techniques in three-dimensional topological insulators in the so-called Majorana regime. We discuss thereafter how the pairing relations in the different regimes can be observed in the tunneling conductance of an *s*-wave proximised three-dimensional topological insulator. We discuss the necessity to incorporate a ferromagnetic insulator to localise the zero-energy bound state to the interface as a Majorana mode.

Keywords: topological insulator, proximised superconductivity, Green functions, odd-frequency, topological regimes, bound states, conductance spectra

S Online supplementary data available from stacks.iop.org/JPhysCM/27/315701/mmedia

(Some figures may appear in colour only in the online journal)

The search for a qubit that is robust against local decoherence has led to extensive studies of the so-called Majorana zero-energy mode in materials with strong spin–orbit coupling (SOC) combined with *s*-wave superconductors. Nanowires and topological insulators are promising candidate materials with strong spin–orbit coupling [1–15]. Experimentalists have already reported signatures of the Majorana zero-energy mode [16–18], where zero-bias conductance peaks are the main features observed in this context.

Besides the possibility of hosting Majorana modes, topological materials are also interesting for the study of unconventional *p*-wave superconductivity by itself. *p*-wave superconductivity gained renewed interest after the prediction that the *p*-wave pairing symmetry in He^3 would lead to half-quantum vortices with potential application to the field of quantum computing [19–21]. Sr_2RuO_4 is believed to have *p*-wave symmetry and together with the prediction of the existence of a nodal gap it has led to an extensive study of this material [22–29]. Also, superconductor/ferromagnet/superconductor junctions are studied for their prospective to switch from a dominant *s*-wave state to a *p*-wave state [30–35]. Furthermore, these devices have potential application

to quantum computation, through which the understanding of the behaviour of *p*-wave superconductivity has become a field on its own.

In this paper we study the *s* and *p*-wave correlations that exist in three-dimensional topological insulators (3D TIs). We first discuss in which regime a dominant *p*-wave correlation is present and under which conditions a dominant *p*-wave correlation can lead to a zero-energy Majorana bound state. We derived the expressions for the bound states formed at a 3D TI in the 'Majorana' regime. We show the relation between odd-frequency pairing and Majorana zero-energy modes by using a Green function approach. We use those new insights to calculate the conductance spectra of proximity induced superconducting 3D TIs with and without broken time-reversal symmetry. The main focus is to understand how the modelled tunneling conductance spectra arise from the *s* and *p*-wave correlations. We will see that the combination of a zero-bias conductance peak together with conductance dips at the gap energy are distinguished features for *p*-wave correlations. We demonstrate that it is not necessary to be in the 'Majorana' regime in order to observe signatures of the *p*-wave correlations.

1. Pairing wave function and Majorana-modes in a 3D TI

In order to determine the pairing relations for a material with strong SOC we start with the relation $[E-H]\mathbf{G}=\mathbb{1}$ where $\mathbf{G}$ is the Green function of the system, $\mathbb{1}$ the identity matrix and H is in the basis $[\psi_\uparrow,\psi_\downarrow,\psi_\downarrow^\dagger,\psi_\uparrow^\dagger]$ [6]. For a system with spin orbit coupling $[E-H]$ is given by

$$\begin{bmatrix} E+\epsilon_p+M & -\lambda_x k_x-\mathrm{i}\lambda_y k_y & 0 & -\Delta \\ -\lambda_x k_x+\mathrm{i}\lambda_y k_y & E+\epsilon_p-M & \Delta & 0 \\ 0 & \Delta & E-\epsilon_p-M & -\lambda_x k_x+\mathrm{i}\lambda_y k_y \\ -\Delta & 0 & -\lambda_x k_x-\mathrm{i}\lambda_y k_y & E-\epsilon_p+M \end{bmatrix}, \tag{1}$$

where $\epsilon_p=\mu-\frac{\hbar k^2}{2m}$. Here, $\lambda_{x,y}$ is the SOC strength in the x and y-directions. At the end we will set the SOC strength equal to the Fermi velocity and $\epsilon_p=\mu$ to discuss the superconducting correlations in the topological surface states. μ is the chemical potential, Δ is the induced superconducting gap and M is the energy of a perpendicular magnetic field, either externally applied (Zeeman term) or due to an exchange interaction. Note that the Zeeman contribution of a magnetic field can be considerable due to the large *g*-factor of the most relevant materials. We neglect the orbital contribution of the applied field.

By taking the inverse of this matrix equation we can obtain the Green function $\mathbf{G}$ expressed as

$$\begin{bmatrix} G_{11} & G_{12} \\ G_{21} & G_{22} \end{bmatrix}. \tag{2}$$

The elements G_{ij} are blocks of 2×2 matrices. The diagonal blocks describe the propagation of the electrons and holes separately. The off-diagonal blocks describe the combined electron and hole propagation, i.e. they describe the propagation of the Cooper pairs in the *s*-wave proximised topological insulator, which is the quantity of interest in this paper. When we represent

$$E-H(\boldsymbol{k})=\begin{bmatrix} \hat{a} & \hat{b} \\ \hat{c} & \hat{d} \end{bmatrix}, \tag{3}$$

the Green function is given by

$$\mathbf{G}(\boldsymbol{k},E)=\begin{bmatrix} (\hat{a}-\hat{b}\ \hat{d}^{-1}\ \hat{c})^{-1}\ (\hat{c}-\hat{d}\ \hat{b}^{-1}\ \hat{a})^{-1} \\ (\hat{b}-\hat{a}\ \hat{c}^{-1}\ \hat{d})^{-1}\ (\hat{d}-\hat{c}\ \hat{a}^{-1}\ \hat{b})^{-1} \end{bmatrix}. \tag{4}$$

We find

$$\begin{aligned} G_{12}=\mathrm{i}\frac{\Delta}{Z}[&(E^2-B_{k,M})\hat{\sigma}_0+2(-\lambda_x k_x\epsilon_p+\mathrm{i}\lambda_y k_y M)\hat{\sigma}_1 \\ &-2(-\lambda_y k_y\epsilon_p-\mathrm{i}\lambda_x k_x M)\hat{\sigma}_2-2ME\hat{\sigma}_3]\hat{\sigma}_2, \end{aligned} \tag{5}$$

with

$$\begin{aligned} Z=&-(E^2-B_{k,M})^2-4(-\lambda_x k_x\epsilon_p+\mathrm{i}\lambda_y k_y M)^2 \\ &-4(-\lambda_y k_y\epsilon_p-\mathrm{i}\lambda_x k_x M)^2-4E^2M^2, \end{aligned} \tag{6}$$

and

$$B_{k,M}=\epsilon_p^2+\Delta^2+(\lambda_x k_x)^2+(\lambda_y k_y)^2-M^2 \tag{7}$$

To discuss the symmetry of the anomalous Green functions, we use the Matsubara representation which can be obtained by analytical continuation, $E+\mathrm{i}\delta\to\mathrm{i}\omega_n$,

$$\begin{aligned} G_{12}=\mathrm{i}\frac{\Delta}{Z}[&(-\omega_n^2-B_{k,M})\hat{\sigma}_0+2(-\lambda_x k_x\epsilon_p+\mathrm{i}\lambda_y k_y M)\hat{\sigma}_1 \\ &-2(-\lambda_y k_y\epsilon_p-\mathrm{i}\lambda_x k_x M)\hat{\sigma}_2-\mathrm{i}2M\omega_n\hat{\sigma}_3]\hat{\sigma}_2 \\ \equiv\ &\mathrm{i}(f_0+\boldsymbol{f}\cdot\boldsymbol{\sigma})\hat{\sigma}_2, \end{aligned} \tag{8}$$

$$\begin{aligned} Z=&-(-\omega_n^2-B_{k,M})^2-4(-\lambda_x k_x\epsilon_p+\mathrm{i}\lambda_y k_y M)^2 \\ &-4(-\lambda_y k_y\epsilon_p-\mathrm{i}\lambda_x k_x M)^2+4\omega_n^2M^2, \end{aligned} \tag{9}$$

$$f_0(\boldsymbol{k},\mathrm{i}\omega)=\frac{\Delta}{Z}(-\omega_n^2-B_{k,M}), \tag{10}$$

$$f_1(\boldsymbol{k},\mathrm{i}\omega)=2\frac{\Delta}{Z}(-\lambda_x k_x\epsilon_p+\mathrm{i}\lambda_y k_y M), \tag{11}$$

$$f_2(\boldsymbol{k},\mathrm{i}\omega)=-2\frac{\Delta}{Z}(-\lambda_y k_y\epsilon_p-\mathrm{i}\lambda_x k_x M), \tag{12}$$

$$f_3(\boldsymbol{k},\mathrm{i}\omega)=-2\mathrm{i}\frac{\Delta}{Z}M\omega_n. \tag{13}$$

The total wave function of a pair of fermions should be asymmetric and the total wave functions can be described by the product of an orbital (or parity), spin and frequency term. Even-frequency pairing means that a function is even in ω_n. If we consider singlet (which is an odd function under

spin permutation) s-wave (orbitally symmetric) pairing, the pairing wave function $F(=G_{12})$ should satisfy the relation $F_s(k) = F_s(-k)$ in order for the wave function to be antisymmetric when the pairing is even in frequency. For p-wave triplet pairing the relation $F_p(k) = -F_p(-k)$ applies [36].

We note that Z is an even function of ω_n and is an even-parity function. The singlet component f_0 belongs to the even-frequency even-parity class (ESE). The two equal-spin components (f_1 and f_2) are even-frequency spin-triplet odd-parity class (ETO). Finally, f_3 belongs to odd-frequency spin-triplet even-parity class (OTE).

For a 3D topological insulator ϵ_p and the SOC strength in the x and y-direction in equation (1) are equal to μ and the Fermi velocity v, respectively. The matrix $[E-H]$ in the relation $[E-H]\mathbf{G} = \mathbb{1}$ is then given by

$$\begin{bmatrix} E+\mu-M & -v|k|e^{i\theta} & 0 & -\Delta \\ -v|k|e^{-i\theta} & E+\mu+M & \Delta & 0 \\ 0 & \Delta & E-\mu+M & -v|k|e^{-i\theta} \\ -\Delta & 0 & -v|k|e^{i\theta} & E-\mu-M \end{bmatrix}, \quad (14)$$

where M is a magnetisation term and θ is the angle between k_x and k_y. It is instructive to compare the 3D TI with semiconductors with strong spin–orbit coupling. Although there are analogies between them, also several differences exist between them. For comparison, we show therefore the model for nanowires in the supplementary material (stacks.iop.org/JPhysCM/27/315701/mmedia).

We assume in this section that $\mu > E_{DP}$ where DP stands for the Dirac point, but the opposite 'hole' regime of $\mu < E_{DP}$ can also easily be obtained. For a chemical potential far above the Dirac point we can make additionally the assumption that $\mu \gg \Delta$. If we also consider low energy excitations we obtain for the topological insulator

$$G_{12} = \begin{bmatrix} F_{\uparrow\uparrow} & F_{\uparrow\downarrow} \\ F_{\downarrow\uparrow} & F_{\downarrow\downarrow} \end{bmatrix}, \quad (15)$$

where

$$\begin{aligned} F_{\uparrow\uparrow} &\sim 2\Delta|k|ve^{i\theta}(M+\mu)/Z_{TI}, \\ F_{\uparrow\downarrow} &\sim \Delta(M^2 - |k|^2v^2 - \mu^2)/Z_{TI}, \\ F_{\downarrow\uparrow} &\sim -\Delta(M^2 - |k|^2v^2 - \mu^2)/Z_{TI}, \\ F_{\downarrow\downarrow} &\sim 2\Delta|k|ve^{-i\theta}(M-\mu)/Z_{TI}, \\ Z_{TI} &= -B_{TI}^2 - 4(-vk_x\mu - ivk_yM)^2 - 4(-vk_y\mu + ivk_xM)^2, \end{aligned} \quad (16)$$

$$B_{TI}^2 = (\mu^2 + v^2|k|^2 - M^2)^2 + 2\Delta^2(\mu^2 + v^2|k|^2 - M^2). \quad (17)$$

G_{21} is related to G_{12} by complex conjugation. The $e^{\pm i\theta}$ factor shows the chiral p-wave character of an s-wave proximised 3D topological insulator.

For the moment we assume that we have even-frequency symmetry. (f_3 in equation (15) can be neglected in the regime of low energy excitations. The appearance of non-negligible odd-frequency symmetry terms will be discussed in section 3).

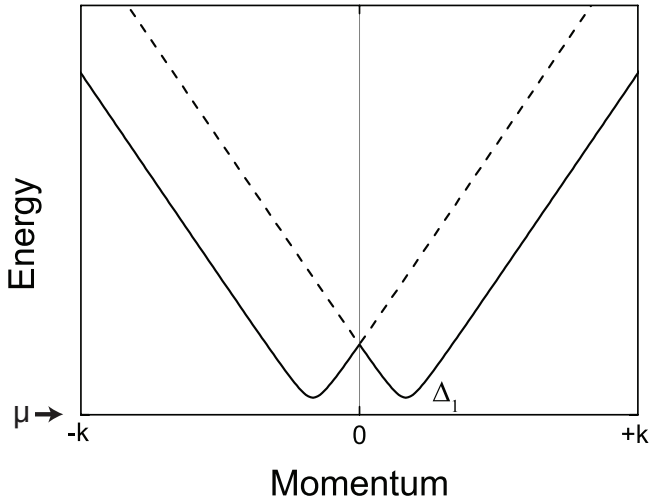

Figure 1. Energy dispersion relation for a 3D topological insulator in the regime $|M| \ll \mu$. The solid line corresponds to $\sqrt{E_{t'} - 2\sqrt{E_{s'}}}$ and the dashed line to $\sqrt{E_{t'} + 2\sqrt{E_{s'}}}$. The graph is plotted for Δ in the order of μ for clarity.

The second and third relations in equation (16), therefore, correspond to s-wave pairing and the other two with p-wave pairing relations.

The energy dispersion relation of the s-wave proximised topological insulator can be obtained by diagonalising the corresponding Hamiltonian as described above, and is found to be

$$E = \pm\sqrt{E_{t'} \pm 2\sqrt{E_{s'}}} \quad (18)$$

where $E_{t'} = M^2 + \Delta^2 + \mu^2 + |k|^2v^2$ and $E_{s'} = M^2\Delta^2 + M^2\mu^2 + |k|^2v^2\mu^2$. In the limit of $\mu \gg \Delta$ this can in good approximation be written as

$$E = \pm\mu \pm \sqrt{v^2|k|^2 + M^2},$$

Now we have all the formal work done to consider the pairing symmetry in three different regimes: $|M| = 0$, $M < \mu$ and the 'Majorana' regime.

1.1. Regime $|M| = 0$

Assume a homogenous magnetisation term (for example caused by an external magnetic field). In the regime $|M| \ll \mu$ we have the situation as depicted in figure 1. There is a gap opening indicated by Δ_1 at positive momentum. At negative momentum a gap with the same size opens. Using the approached dispersion relation we have $\mu = v|k|$ at the gap opening. Substituting this relation into equation (16) we obtain the following anomalous Green function relations at Δ_1

$$\begin{aligned} F_{\uparrow\uparrow} &\sim 2\Delta|k||k_f|e^{i\theta}/Z_{TI}, \\ F_{\uparrow\downarrow} &\sim -2\Delta|k|^2/Z_{TI}, \\ F_{\downarrow\uparrow} &\sim 2\Delta|k|^2/Z_{TI}, \\ F_{\downarrow\downarrow} &\sim -2\Delta|k||k_f|e^{-i\theta}/Z_{TI}. \end{aligned}$$

We see from the above that the matrix elements corresponding to the *s*-wave pairing are in magnitude as large as the matrix elements corresponding to the *p*-wave relations. So in the case of negligible M we have an equal admixture of *s*-wave and *p*-wave correlations. This result is similar to the result found by Tkachov in [37, 38] for a topological insulator. In [15] Fu and Kane transform to another basis, $c_k = (\psi_{\uparrow k} + e^{i\theta}\psi_{\downarrow k})$, in which the Hamiltonian becomes equivalent to a spinless $p_x + ip_y$ (dominant *p*-wave). Although this transformation is an elegant way to show that *p*-wave relations are present, when doing predictions for the experimental outcome in this basis, a transformation also has to be made to the *s*-wave superconductor deposited on top. This would also cause an additional phase shift in the normal superconductor through which one can then conclude that the *p*-wave is no longer dominant. Nonetheless, the existing proposals of Fu and Kane for Majorana devices [15] still hold as it was already noted that breaking time-reversal symmetry can make $p_x + ip_y$ dominant, as we will see next.

1.2. Regime $M < \mu$

As we turn on the perpendicular magnetisation term, it follows from the dispersion relations that we have at $\Delta_\downarrow$, $\mu^2 = v^2|k|^2 + M^2$. The anomalous Green function relations become

$$F_{\uparrow\uparrow} \sim 2\Delta e^{i\theta}\sqrt{(\mu - M)(\mu + M)^3}/Z_{\mathrm{TI}},$$
$$F_{\uparrow\downarrow} \sim -2\Delta(\mu^2 - M^2)/Z_{\mathrm{TI}},$$
$$F_{\downarrow\uparrow} \sim 2\Delta(\mu^2 - M^2)/Z_{\mathrm{TI}},$$
$$F_{\downarrow\downarrow} \sim -2\Delta e^{-i\theta}\sqrt{(\mu - M)^3(\mu + M)}/Z_{\mathrm{TI}}.$$

As soon as the time-reversal symmetry is broken the increase in M causes the *p*-wave component to become larger in magnitude than the *s*-wave component. This can be intuitively understood by notifying that a magnetic field aligns the spins parallel to the field. Therefore spin triplet pairing is favoured above spin singlet pairing. It is therefore possible to already observe dominant *p*-wave features in the regime $M < \mu$.

1.3. The 'Majorana' regime

Unfortunately, the presence of dominant *p*-wave correlations still does not mean that a Majorana zero-energy mode exists as soon as we apply magnetisation, because the zero-energy mode is not yet fully localised. As already noted by Fu and Kane [15], the 2D TI surface has no edge, which prevents a localised Majorana bound state to form. The same is true in a 2D topological insulator, where 1D edge states can go around the 2D topological insulator. We therefore need a different device in order to localise the zero-energy mode.

One way to create an edge *and* break time-reversal symmetry is shown in figure 2(a). The M denotes the magnetisation induced by the ferromagnet. We assume here that we have an insulating ferromagnet so that the current is only going through the surface states. A different way is to have a Josephson junction with a phase difference between the two superconductors [15]. For now, we focus on the device in figure 2(a). In order to have a localised zero-energy mode, the Majorana mode needs to be localised both at the superconducting side and at the ferromagnet side. At the superconducting side the superconducting gap is doing the job. At the ferromagnet side, the magnetisation has to be large enough such that the Fermi level is inside the gap (see figure 2(b)). Then, the zero-energy mode is fully localised. To be more specific, in order to have a proper localised Majorana mode one has to satisfy the relation $M(x) > \sqrt{\Delta(x)^2 + \mu^2}$ at the ferromagnet side. We also included the superconducting gap as a function of position to take the proximity effect into account.

2. Surface Andreev bound states and Majorana zero-energy modes

So far we have looked at the properties of the bulk, i.e. the inner part of the *s*-wave proximised 2D surface states of the topological insulator. We are now going to discuss the properties at the interface between the superconductor and ferromagnet, where the Majorana zero mode is formed in the Majorana regime. It is expected that different symmetries are present at the surface or edge of a superconducting system, as noted in [39, 40]. Due to a finite size, the translational symmetry is broken in that direction. The orbital symmetry (even or odd) is then not a well-defined parameter anymore, giving rise to mixed odd and even symmetry at the interface. The spin pairing symmetry, however, is not affected by the finite size. The only option, therefore, to have an asymmetric wave function is to allow for odd-frequency states at the interface.

Figure 2(a) shows the superconductor/ferromagnet device needed to localise a Majorana state. In experiments it is useful to use a ferromagnetic *insulator* (FI) to ensure that the magnet itself does not shunt the device [41]. We will, therefore, indicate the ferromagnet as FI in the remaining part of the paper.

Assume that we are in the regime with a fully localised Majorana state, i.e. $M > \mu$. The resulting SABSs can be calculated by considering a small non-superconducting region in the order of the coherence length to model the suppression of the gap near the edge (figure 2(c)). We use the wave functions described in our previous work ([42]) to calculate the SABSs. The direction of the transmitted waves in the superconductor is chosen such that k is conserved parallel to the interface. We assume that the electrons in the non-superconducting part are confined and, therefore, that they completely reflect back at $x = -L$.

The phase difference that is picked up in one round trip (figure 2(c)) is

$$\begin{aligned} &2L(|k_e| - |k_h|) - 2\theta + 3\pi + 2\arccos E/\Delta = 2\pi n \\ &= \frac{4LE}{\hbar v_f \cos\theta} - 2\theta + 3\pi + 2\arccos E/\Delta \end{aligned} \tag{19}$$

so

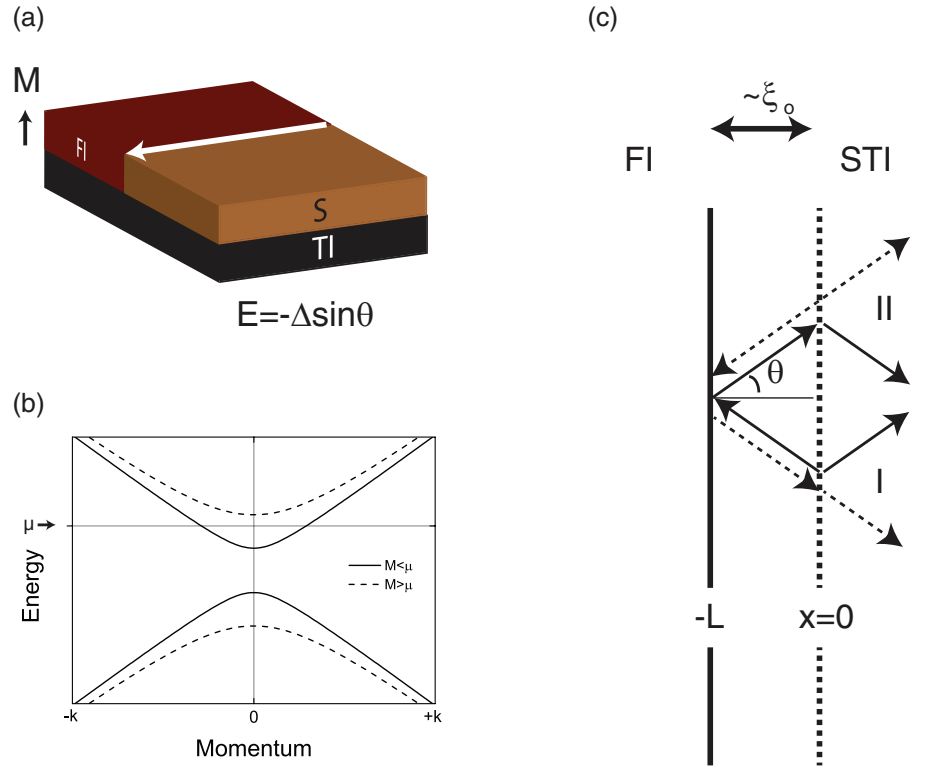

Figure 2. (a) A ferromagnet insulator (FI) can both break time-reversal symmetry and localise the Majorana zero-energy mode in a TI. The location of the Majorana mode is indicated by the white arrow. (b) The dispersion relation of the topological insulator at the ferromagnet side for a magnetisation smaller and larger than the chemical potential. In the former, the chemical potential still lies in the Dirac cone. In the latter, the states around the chemical potential are gapped out and the zero-energy mode is localised at the interface between the superconductor and ferromagnet. (c) Calculation of the surface Andreev bound state. To model the suppression of the superconducting gap of the superconducting topological insulator (STI) we assume a normal part in the order of the coherence length ξ_0 at the interface between the superconductor and the ferromagnet.

$$\frac{E}{\Delta} = \cos\left(-3\pi/2 + \theta + \frac{2LE}{\hbar v_f \cos\theta}\right) \tag{20}$$

$$= -\sin\left(\theta + \frac{2LE}{\hbar v_f \cos\theta}\right). \tag{21}$$

Taking the limit $L \to 0$ we have

$$\frac{E}{\Delta} = -\sin(\theta) \tag{22}$$

$$= -k_y/|k|. \tag{23}$$

When the magnetisation of the FI is in the exact opposite direction, the resulting ABS is $\frac{E}{\Delta} = \sin(\theta)$. This is exactly the SABS of a chiral p-wave superconductor [43].

In order to determine the features of the SABS and its relation to Majorana zero energy modes, we consider the regimes around $E = 0$ and $E \neq 0$ in more detail in the following.

2.1. Around E = 0

In figure 2(c) we can calculate the reflection and transmission coefficients of the electron and holes at the interface by using continuation of the wave function. From these coefficients it follows that the total wave function in the superconducting part in the electron–hole basis $[\psi_{k\uparrow}, \psi_{k\downarrow}, \psi^\dagger_{-k\uparrow}, \psi^\dagger_{-k\downarrow}]$ is given by

$$\Psi = \frac{e^{i\theta}}{\Delta}\begin{pmatrix} (E - i\tilde{\Omega}) \\ -e^{-i\theta}(E - i\tilde{\Omega}) \\ \Delta e^{-i\theta} \\ \Delta \end{pmatrix} e^{-ikr} e^{-r/\xi_0} + \frac{1}{E + i\tilde{\Omega}}\begin{pmatrix} (E + i\tilde{\Omega}) \\ (E + i\tilde{\Omega})e^{i\theta} \\ -\Delta e^{i\theta} \\ \Delta \end{pmatrix} e^{ikr} e^{-r/\xi_0}, \tag{24}$$

where $\tilde{\Omega} = \sqrt{\Delta^2 - E^2}$ and $\xi_0 = \sqrt{\Delta^2 - E^2}/v_F$. Around $E = 0$ (and so around $\theta = 0$) the expression for the Majorana zero mode becomes

$$\Psi = e^{-x/\xi_0}\begin{pmatrix} 2e^{-i\pi/4}\cos(kx + \pi/4) \\ 2e^{i\pi/4}\cos(kx - \pi/4) \\ 2e^{i\pi/4}\cos(kx + \pi/4) \\ 2e^{-i\pi/4}\cos(kx - \pi/4) \end{pmatrix}. \tag{25}$$

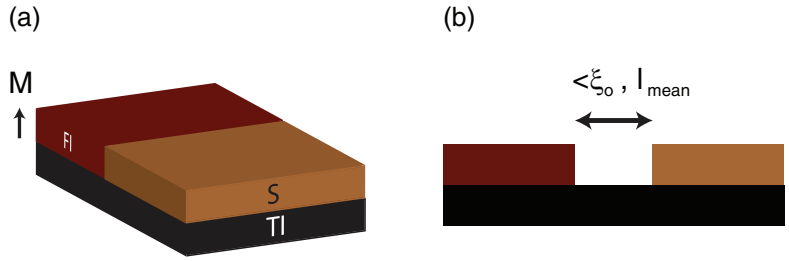

Figure 3. (a) In the calculation of the conductance we consider two electrodes: the proximised TI by the FI and the proximised TI by the *s*-wave superconductor. (b) In order for the Andreev formalism to hold, the distance between the FI and the superconductor should be smaller than the mean free path and the coherence length.

Note that this expression is consistent with the result found by Tanaka and Asano in a semiconductor/superconductor device [6]. In their case, an additional magnetic field is applied through which only the spin up part survives of equation (25).

To give a complete picture of the properties of this Majorana zero-energy mode, we calculated the frequency symmetry of this zero-energy state. The anomalous Green function can be obtained by the relation

$$F(E,r,r';\theta)_{\uparrow\downarrow} = \Sigma_n \left[\frac{u_{n\uparrow}(r)v^*_{n\downarrow}(r')}{E+\mathrm{i}\delta-E_n} + \frac{v^*_{n\uparrow}(r)u_{n\downarrow}(r')}{E+\mathrm{i}\delta+E_n} \right]. \tag{26}$$

Where u and v are the electron and hole parts, respectively. The relationship at $x = x' = 0$ satisfies

$$\overline{F}_{\beta,\alpha}(\mathbf{r},E,\mathbf{p}) = -[F_{\alpha,\beta}(\mathbf{r}-E,\mathbf{p})]^* \tag{27}$$

where $\bar{F}$ denotes the conjugated of F and α and β are the spin-indices [36], which means the Cooper pairs are odd-frequency pairs. The spatial symmetry of equation (25) satisfies the *s*-wave symmetry. Therefore, the boundary of a pure *p*-wave even-frequency superconductor is a pure *s*-wave, odd-frequency state. The appearance of odd-frequency states near zero-energy is also noted in calculations on p_x and $p_x + \mathrm{i}p_y$ superconductors [44].

2.2. $E \neq 0$

In a similar way as discussed for zero energy we can calculate the anomalous Green function for energies larger than zero. We find that there is an admixture between even and odd-frequency. The odd and even-frequency parts are, respectively, given by

$$F_{\mathrm{odd}} \backsim \sqrt{1-E^2/\Delta^2}\,, \tag{28}$$

$$F_{\mathrm{even}} \backsim E/\Delta. \tag{29}$$

Near zero-energy, the odd-frequency part is dominant and the even-frequency contribution grows with E. The emergence of a (partly) odd-frequency amplitude at the surface/interface due to spatial non-uniformity [39, 45–47] or interorbital pairing [48] is well-known for superconducting systems. However, in this case, we have a full odd-frequency state at zero energy. Therefore, the conclusion of Asano and Tanaka [6] holds that in these devices pure odd-frequency Cooper pairs and the Majorana zero-energy mode are one and the same thing.

3. TI/STI tunneling conductance

In the study of the conductance we consider the system where one electrode consists of the topological insulator proximised by the FI and the other electrode of the topological insulator proximised by the *s*-wave superconductor, as depicted in figure 3(a). We assume here that the magnetisation is smaller than the chemical potential in the magnetic topological insulator electrode. We modelled this magnetic TI/STI interface by using the wave functions in the magnetic TI and STI, as described in [42], and match them at the interface such that

$$\psi_{in} + a\psi_h + b\psi_e = t_e\psi_{Se} + t_h\psi_{Sh} \tag{30}$$

where ψ_h is the reflected hole, ψ_e the reflected electron, ψ_{Se} the transmitted quasi-particle in the electron branch of the superconductor, ψ_{Sh} the transmitted quasi-particle in the hole branch of the superconductor and a, b, t_e and t_h are the Andreev, normal, electron transmission and hole transmission coefficients, respectively. We calculated then the conductance by using the relation

$$\frac{G}{G_0} = \frac{\int_{-\pi/2}^{\pi/2} \mathrm{d}\theta \cos(\theta) T(\theta, \mathrm{eV})}{\int_{-\pi/2}^{\pi/2} \mathrm{d}\theta \cos(\theta) T(\theta, \mathrm{eV})\big|_{\Delta=0}}, \tag{31}$$

where $T(\theta,E) = 1+|a|^2-|b|^2$ and θ is the angle between k_x and k_y. The Andreev formalism holds when the distance between the superconducting and the ferromagnet side is smaller than the coherence length and the mean free path (l_{mean}), as shown in figure 3(b). We choose here to divide the conductance by the energy dependent normal conductance to ensure that the normalised conductance goes to one at high voltage.

We first consider the case with time-reversal symmetry, i.e. without the FI on top of the TI. By means of a gate electric field, the chemical potential at the superconductor side can be tuned independently from the non-superconductor side. Therefore, we make from now on a distinction between the chemical potential at the superconductor and non-superconductor side. In figure 4(a) we plotted the normalised conductance for different ratios of the STI chemical potential, μ_{S}, and TI chemical potential, μ_{TI}. A conductance peak at $\mathrm{eV} = \Delta$ appears for larger barriers due to Andreev resonance at this energy, similar to the *s*-wave case. Opposite to the *s*-wave case, the value of the conductance never drops to zero, even for a large mismatch where the barrier height goes practically

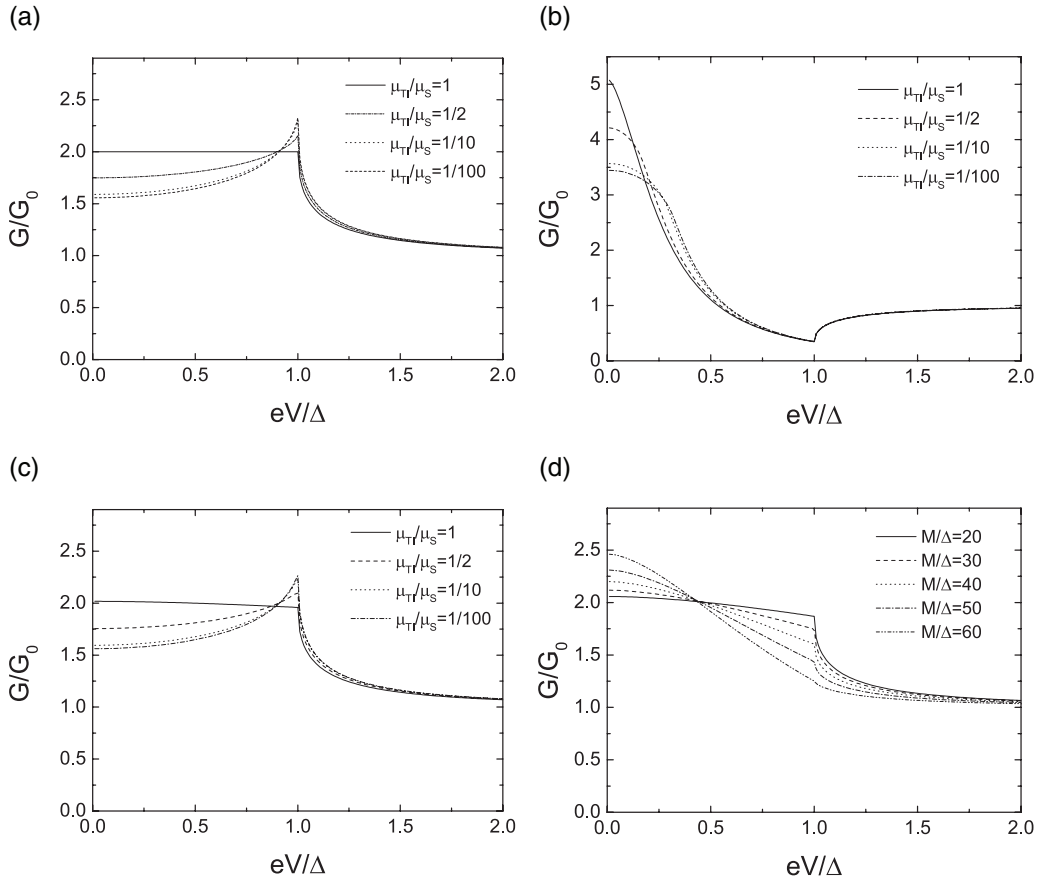

Figure 4. (a) Conductance spectra for a TI/STI configuration for different mismatches in chemical potential. (b) Conductance spectra for a magnetisation $M/\Delta = 95$, $\mu_{\mathrm{TI}}/\Delta = 100$ and different mismatches in chemical potential. (c) Conductance spectra for a magnetisation $M/\Delta = 10$, $\mu_{\mathrm{TI}}/\Delta = 100$ and different mismatches in chemical potential. (d) The conductance spectra for different values of magnetisation and $\mu_{\mathrm{TI}}/\Delta = \mu_{\mathrm{S}}/\Delta = 100$. Even if the magnetisation is smaller than the chemical potential, clear signatures of the SABSs are still visible.

to infinity ($\mu_{\mathrm{S}}/\mu_{\mathrm{T}} = 1/100$). The conductance inside the gap is close to one instead, which can be understood by considering different angles of incidence. The large barrier causes the propagation direction in the superconductor to be almost equal to $\theta = 0$ as follows from the conservation of parallel momentum: $\theta_{\mathrm{S}} = \arcsin(\sin\theta\mu_{\mathrm{TI}}/\mu_{\mathrm{S}})$. The spin in the topological insulator with $\theta = 0$ sees no barrier because of Klein tunneling (which gives perfect Andreev reflection for all energies) and for $\theta = \pi/2$ the spin mismatch is the largest, which results in the lowest transparency (perfect normal reflection). For angles in between, the transparency of the barrier increases continuously from one to zero for an increasing angle of incidence. The angle averaged conductance is therefore close to one.

The presence of a non-zero conductance for energies below the gap, even for large barriers, distinguishes the proximised TI surface from conventional *s*-wave symmetry superconductors. Although the *p*-wave pairing is not dominant in the time symmetric situation, the *p*-wave correlations are encoded in the non-zero conductance for energies below the gap in the presence of a barrier. The fact that the gap does not go to zero is due to the spin-momentum locking, which is also responsible for the *p*-wave correlations.

4. TI/STI tunneling conductance with broken time-symmetry

To modulate the TI/STI tunneling conductance with broken time-reversal symmetry we take the set-up, as displayed in figure 3(a). We will use a relatively large chemical potential compared to the superconducting gap to model the experimentally realistic regime. The topological insulators so far have the Dirac point close or at the same energy as the bulk bands so as long as the chemical potential is in the gap, the chemical potential is likely much larger than the superconducting gap. We argued in earlier work [42], that a magnetisation in the case of a ferromagnet insulator will only be a few percent of the chemical potential. However, to see the effect of the broken time-symmetry we also modulated the conductance spectrum for a magnetisation value of 0.95 μ_{TI}. This result is shown in figure 4(b). There are two distinguished features compared to an N/S interface, namely a zero-bias peak (ZBP) and a conductance dip at $\mathrm{eV} = \Delta$. The appearance of these two features for large magnetisation is also reported by Linder *et al* [41]. Both features are due to the formation of SABSs at the interface. In fact, the SABSs have a constant density of states at energies between $-\Delta$ and

$+\Delta$ as follows from equation (22), but from conservation of parallel momentum it follows that the angles near zero have a larger transparency. The coherence peaks at the gap energy in the low barrier limit are replaced by resistance peaks at the same energy. The coherence dips at Δ arise from the spectral weight transfer from high to low energy due to the formation of SABSs. This results in a decrease of the density of states at Δ. Therefore, next to a zero bias conductance peak, coherence dips are also a distinguished feature of a *p*-wave order parameter compared to *s*-wave.

Note that the surface states are not fully gapped yet with a magnetisation of 95% of the chemical potential, i.e. the chemical potential is not inside the gap at the FI side. We are therefore not in the topologically non-trivial regime. However, the increased reflection at the interface or enhanced *p*-wave pairing symmetry due to magnetisation causes the SABS to form at the interface. If we use a magnetisation value of 10% of the chemical potential in the TI, figure 4(c) is obtained. We see there is only a small effect on the conductance spectra around zero energy at Δ compared to the time-reversal symmetry case in figure 4(a). Figure 4(d) shows the effect of increasing the magnetisation for $\mu_{\mathrm{TI}} = \mu_{\mathrm{S}} = 100\Delta$. Gradually, the conductance at zero energy increases while at Δ the conductance decreases due to the formation of SABSs for larger magnetisation. It shows that the ZBP and conductance dip at the gap energy come together. That is, if one has a dominant *p*-wave pairing wave function and if one observes a ZBP, then the conductance dips are also present. As soon as the ZBP becomes less pronounced, as is the case for lower magnetisations, the conductance dip at $\mathrm{eV} = \Delta$ is less pronounced. The observation of *both* a ZBP and a conductance dip is a strong signature for a *p*-wave state. For practical ferromagnets that have a magnetisation in the order of a few percent of the chemical potential of the TI, it is not expected to see this particular *p*-wave signatures back in the conductance spectra. A pronounced deviation from *s*-wave behaviour starts to occur when $M/\Delta = 60$ (see figure 4(d)). With a typical exchange energy of 40 meV [49, 50] it means that one has to gate tune the chemical potential to about 70 meV from the Dirac point, which seems doable experimentally [51, 52].

5. Discussion and conclusion

An equal admixture of *s* and *p*-wave correlations exists in a 3D topological insulator proximised by an *s*-wave superconductor. By inducing a perpendicular magnetisation, the *p*-wave pairing becomes dominant. For a magnetisation energy as large as the chemical potential, the topological regime is entered with Majorana modes.

We studied the symmetry of the bound state of a 3D topological insulator in the Majorana regime. Green function techniques show us that the pure odd-frequency pairing state at interfaces is equivalent to a zero-energy Majorana mode.

In the conductance spectra the increasing *p*-wave pairing can be observed by the presence of a ZBP together with a conductance dip at the gap energy. In the time-reversal symmetric case, the non-zero sub-gap conductance in the presence of large interface barriers, indicates that *p*-wave correlations are present.

Acknowledgments

We acknowledge insightful discussions with M P Stehno, Y Tanaka and E M Hankiewicz. This work is supported by the Netherlands Organization for Scientific Research (NWO), by the Dutch Foundation for Fundamental Research on Matter (FOM), the European Research Council (ERC) and supported in part by the Russian Science Foundation, project N 15-12-30030 and partially supported by 'Topological Quantum Phenomena' (Grant No. 22103002) Grant-in Aid for Scientific Research on Innovative Areas, KAKENHI (Grant No. 26287069) from the Ministry of Education, Culture, Sports, Science and Technology (MEXT) of Japan.

References

[1] Sau J D, Luthchyn R M, Tewari S and Das Sarma S 2010 *Phys. Rev. Lett.* **104** 040502
[2] Alicea J 2010 *Phys. Rev.* B **81** 125318
[3] Oreg Y, Refael G and von Oppen F 2010 *Phys. Rev. Lett.* **105** 177002
[4] Lutchyn R M, Sau J D and Das Sarma S 2010 *Phys. Rev. Lett.* **105** 077001
[5] Pikulin D I, Dahlhaus J P, Wimmer M, Schomerus H and Beenakker C W J 2012 *New J. Phys.* **14** 125011
[6] Asano Y and Tanaka Y 2013 *Phys. Rev.* B **87** 104513
[7] Alicea J, Oreg Y, Refael G, von Oppen F and Fisher M P A 2011 *Nat. Phys.* **7** 412
[8] Stanescu T D and Tewari S 2013 *J. Phys.: Condens. Matter* **25** 233201
[9] Akhmerov A R, Nilsson J and Beenakker C W J 2009 *Phys. Rev. Lett.* **102** 216404
[10] Qi X-L and Zhang S-C 2011 *Rev. Mod. Phys.* **83** 1057–110
[11] Linder J, Tanaka Y, Yokoyama T, Sudbo A and Nagaosa N 2010 *Phys. Rev. Lett.* **104** 067001
[12] Tanaka Y, Yokoyama T and Naoto N 2009 *Phys. Rev. Lett.* **103** 107002
[13] Fu L and Kane C L 2009 *Phys. Rev.* B **79** 161408
[14] Fu L and Kane C L 2009 *Phys. Rev. Lett.* **102** 216403
[15] Fu L and Kane C L 2008 *Phys. Rev. Lett.* **100** 096407
[16] Deng M T, Yu C L, Huang G Y, Larsson M, Caroff P and Xu H Q 2012 *Nano Lett.* **12** 6414
[17] Mourik V, Zuo K, Frolov S M, Plissard S R, Bakkers E P A M and Kouwenhoven L P 2012 *Science* **336** 1003–7
[18] Das A, Ronen Y, Most Y, Oreg Y, Heiblum M and Shtrikman H 2012 *Nat. Phys.* **8** 887–95
[19] Osheroff D D, Richardson R C and Lee D M 1972 *Phys. Rev. Lett.* **28** 885
[20] Osheroff D D, Gully W J, Richardson R C and Lee D M 1972 *Phys. Rev. Lett.* **29** 920
[21] Leggett A J 1972 *Phys. Rev. Lett.* **29** 1227
[22] Ishida K, Mukuda H, Kitaoka Y, Asayama K, Mao Z Q, Mori Y and Maeno Y 1998 *Nature* **396** 658–60
[23] Luke G M *et al* 1998 *Nature* **394** 558–61
[24] Agterberg D F 1998 *Phys. Rev. Lett.* **80** 5184
[25] Kealey P G *et al* 2000 *Phys. Rev. Lett.* **84** 6094
[26] Duffy J A, Hayden S M, Maeno Y, Mao Z, Kulda J and McIntyre G J 2000 *Phys. Rev. Lett.* **85** 5412
[27] Eremin I, Manske D, Ovchinnikov S G and Annett J F 2004 *Ann. Phys.* **13** 149–74

[28] Kallin C and Berlinsky A J 2009 *J. Phys.: Condens. Matter* **21** 164210
[29] Kallin C 2012 *Rep. Prog. Phys.* **75** 042501
[30] Ryazanov V V, Oboznov V A, Veretennikov A V, Rusanov A Y, Golubov A A and Aarts J 2001 *Phys. Rev. Lett* **86** 2427
[31] Golubov A A, Kupriyanov M Y and Fominov Y V 2002 *JETP Lett.* **75** 190
[32] Matsuda K-I, Akimoto Y, Uemura T and Yamamoto M 2009 *J. Phys.: Conf. Ser.* **150** 052155
[33] Samokhvalov A V, Shekhter R I and Buzdin A I 2014 *Sci. Rep.* **4** 5671
[34] Buzdin A I 2005 *Rev. Mod. Phys.* **77** 935
[35] Bergeret F S, Volkov A F and Efetov K B 2005 *Rev. Mod. Phys.* **77** 1321
[36] Tanaka Y and Golubov A A 2007 *Phys. Rev. Lett.* **98** 037003
[37] Tkachov G 2013 *Phys. Rev.* B **87** 245422
[38] Tkachov G and Hankiewicz E M 2013 *Phys. Rev.* B **88** 075401
[39] Tanaka Y, Sato M and Nagaosa N 2012 *J. Phys. Soc. Japan* **81** 011013
[40] Gor'kov L P and Rashba E I 2001 *Phys. Rev. Lett.* **87** 037004
[41] Linder J, Tanaka Y, Yokoyama T, Sudbø A and Nagaosa N 2010 *Phys. Rev.* B **81** 184525
[42] Snelder M, Veldhorst M, Golubov A A and Brinkman A 2013 *Phys. Rev.* B **87** 104507
[43] Eschrig M, Iniotakis C and Tanaka Y 2010 arXiv: 1001.2486
[44] Bakurskiy S V, Golubov A A, Kupriyanov M Y, Yada K and Tanaka Y 2014 *Phys. Rev.* B **90** 064513
[45] Tanaka Y, Golubov A A, Kashiwaya S and Ueda M 2007 *Phys. Rev. Lett.* **99** 037005
[46] Tanaka Y, Tanuma Y and Golubov A A 2007 *Phys. Rev.* B **76** 054522
[47] Eschrig M, Löfwander T, Champel T, Cuevas J C, Kopu J and Schön G 2007 *J. Low Temp. Phys.* **147** 457
[48] Black-Schaffer A M and Balatsky A V 2013 *Phys. Rev.* B **87** 220506
[49] Semenov Y G, Duan X and Kim K W 2012 *Phys. Rev.* B **86** 161406
[50] Kong B D, Semenov Y G, Krowne C M and Kim K W 2011 *Appl. Phys. Lett.* **98** 243112
[51] Kim D, Cho S, Butch N P, Syers P, Kirshenbaum K, Adam S, Paglione J and Fuhrer M S 2012 *Nat. Phys.* **8** 459–63
[52] Yang F, Taskin A A, Satoshi S, Segawa K, Ohno Y, Matsumoto K and Ando Y 2014 *Appl. Phys. Lett.* **104** 161614